Progress In Electromagnetics Research C, Vol. 67, 117–125, 2016

Compact UWB Band-Notch MIMO Antenna with Embedded Antenna Element for Improved Band Notch Filtering

Jun Tao[1] and Quanyuan Feng[2, *]

Abstract—A compact printed ultra-wideband (UWB) multiple-input-multiple-output (MIMO) antenna with embedded structure is proposed. The proposed MIMO antenna consists of two coplanar waveguide-fed (CPW) antenna elements, and the element with smaller size is built in the radiator of the other element. Thus, the compact size, $30 \times 22\,\text{mm}^2$, is completely determined by the larger one, which makes the MIMO antenna have similar size to the conventional single UWB antennas. The antenna elements are fed perpendicularly to achieve superior isolation. A T-shaped parasitic stub, a pair of C-shaped slots, an extended Z-shaped stub and a rectangular slot are employed and each two structures filter the interference for one antenna element. The achieved rejection bands remain relatively stable over the stop-band frequencies and decline rapidly at cut-off frequencies. Thus, the proposed MIMO antenna obtains superior filtering performance. The proposed antenna is fabricated and measured. The measured results indicate that two antenna elements can operate in the impedance bandwidth larger than 3.1–10.6 GHz with notched bands of 5–6 GHz, and the mutual coupling is below −15 dB over the entire UWB frequency spectrum. The proposed MIMO antenna is a competitive candidate for UWB MIMO communication systems.

1. INTRODUCTION

UWB technology is a promising solution for short-range high-speed wireless communication systems due to the characteristics of high transmission rate and low-spectral-density radiated power. Since the Federal Communications Commission (FCC) authorized the unlicensed frequency spectrum of 3.1–10.6 GHz as UWB communication [1], multiple works have been put forward. However, the UWB systems also suffer from the problem of multipath fading. To solve the problem, MIMO technology is employed due to its capability to provide multiplexing gain and diversity gain [2]. Mutual coupling is one of the critical factors that directly affect the performance of the MIMO system. To improve the isolation performance, orthogonally feeding structures, decoupling slots and parasitic branches are common and efficient methods due to their simple structures. In [3–5], the orthogonally feeding structure is prone to introduce the pattern/gain diversity, double polarizations and compact size. The decoupling slots [5, 6], which usually are added between two antenna elements, work as $\lambda_g/4$ resonators. The parasitic branches, in [7, 8], introduce additional current paths to impair the electromagnetic coupling of two ports. The hybrid method, which is composed of aforementioned methods, is extensively employed to enhance the isolation. Moreover, EBG [9] and neutralization line [10] are viable methods to improve isolation. But they are normally complex to design and occupy considerable space.

In addition, some narrowband systems, such as WLAN systems (5.15–5.825 GHz) and Dedicated Short-Range Communication systems (5.85–5.925 GHz), cause electromagnetic interferences for UWB systems. Thus, the rejection band of 5.15–6 GHz is necessary for UWB antennas. To the authors'

Received 19 July 2016, Accepted 4 September 2016, Scheduled 19 September 2016

* Corresponding author: Quanyuan Feng (fengquanyuan@home.swjtu.edu.cn).

[1] The School of Information Science and Technology, Southwest Jiaotong University, Chengdu, China. [2] Institute of Microelectronics, Southwest Jiaotong University, Chengdu, China.

best knowledge, no band-notch UWB MIMO antenna, which possesses relatively stable stop band and sharp cut-off frequencies, has been studied, especially for the antenna combining with different elements. Masses of band-notch structures are proposed, such as [4] and [6]. These structures work as resonators or generate the opposite currents to suppress the radiation. However, almost all of the rejection bands of these proposed UWB MIMO antennas have sharp shapes and decline rapidly out of the center frequencies due to their one-fold resonant frequencies, and thus they cannot achieve good filter characteristics. To improve the filtering performance, two band-notch structures with separate resonant frequencies are employed in each antenna element, and then the filtering performance is improved by the stop bands overlap. However, the size of the proposed MIMO antenna remains unchanged.

At first glance, our proposed antenna has a similar structure to the antenna in [11]. However, the MIMO antenna in [11] is combined with two detached antenna elements divided by a semi-circular slot, and it only covers the lower UWB band of 3.1–5.15 GHz. The size of the antenna is 25 $\times$40 mm^2, and no rejection bands are obtained due to its narrow operation frequency bandwidths. Furthermore, our design processes are quite different from [11]. The processes will be shown in the following sections.

In this paper, a UWB MIMO antenna with compact size of 30 $\times$ 22 mm^2 (only 66% of [11]) is proposed. Owing to the embedded structure, the overall size of the MIMO antenna is completely decided by the larger antenna element, and thus the overall size nearly amounts to a conventional single UWB antenna. Two antenna elements are fed perpendicularly, and then a good isolation (almost all results are below -20 dB) is achieved without extra decoupling structure. Two groups of band-notch structures are introduced to eliminate the interference of 5.15–6 GHz, and each group primarily works for one antenna element. Unlike the conventional UWB MIMO antenna with single stop band notch, in our paper, two different band-notch structures generate adjacent stop bands for antenna element, and thus the proposed MIMO antenna achieves superior filtering performance due to the stop bands overlap. The measured impedance bandwidths of two antenna elements are larger than 3.1–10.6 GHz, and two rejection bands of 5–6 GHz are obtained. The proposed antenna also possesses relatively stable omnidirectional radiation patterns and high radiation efficiency. The measured envelope correlation coefficient is lower than 0.2. Thus, the proposed antenna is a competitive candidate for UWB devices.

2. DESIGN AND ANALYSIS OF THE PROPOSED ANTENNA

The geometry and configuration of the proposed antenna with compact size of 30 $\times$22 mm^2 are shown in Fig. 1(a), and the prototype of the fabricated antenna is depicted in Fig. 1(b). It is printed on an F4b-2 substrate with the relative dielectric constant of 2.65 and thickness of 0.8 mm.

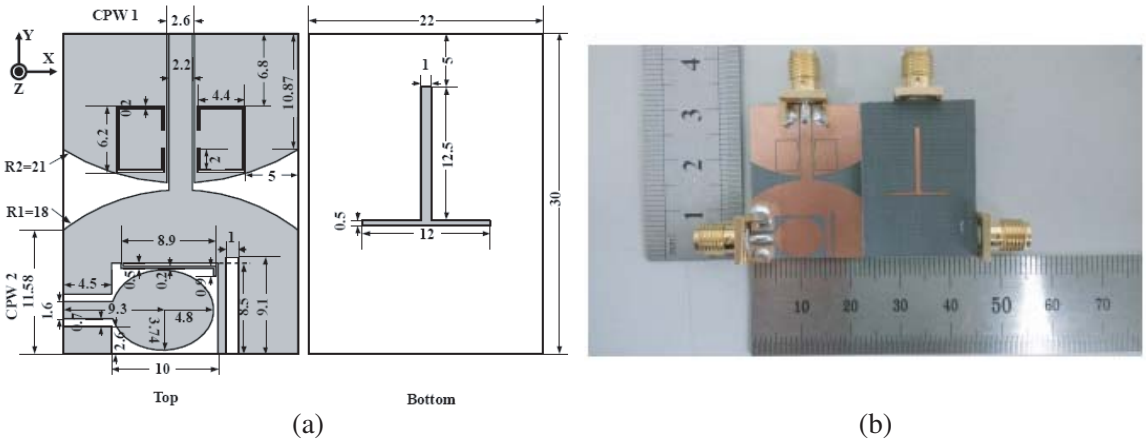

Figure 1. Proposed UWB MIMO antenna. (a) Configuration and geometry of UWB MIMO antenna (UNIT: mm). (b) Fabricated UWB MIMO antenna.

2.1. Antenna Design

The larger antenna element, denoted as CPW 1, is a typical monopole antenna with a coplanar waveguide-fed structure. This simple structure is easy to design and realize wide impedance bandwidth. To satisfy UWB applications, arch-shaped edges are employed in the radiator and ground plane of CPW 1, which helps to generate multiple resonant frequencies and improve impedance matching. The antenna element with smaller size (half-slot antenna), denoted as CPW 2, is embedded in the radiator of CPW 1, and thus the overall size of the proposed MIMO antenna is only decided by CPW 1.

CPW 2 is a half-slot antenna, and its impedance bandwidth is sensitive to the shape of the radiator. A fine-tuned elliptical radiator, which possesses the major semi-axis of 4.8 mm and minor semi-axis of 3.74 mm, is obtained through multiple experiments and optimizations. Due to size constraints of the paper, the optimization processes of the elliptical radiator are not shown in the paper. Feeding stripline width of CPW 1/CPW 2 is modified to be 2.2/1.6 mm, and the gap width is 0.2/0.7 mm for matching 50-Ω characteristic impedance. Two antenna elements are fed perpendicularly to each other to achieve superior isolation. In order to eliminate the interferences of narrowband communication systems, two groups of band-notch structures are introduced. One group includes a T-shaped parasitic stub and a pair of C-shaped slots, and the other group includes a Z-shaped extended branch and a rectangular slot. Each group primarily works for one antenna element.

To decrease the errors of SMA connecter, the SMA models are employed in the simulations. The electromagnetic solvers, Ansoft HFSS and CST, are utilized for antenna design and parameters optimizations.

2.2. The Effects of CPW 2 on CPW 1

The original model of CPW 1, denoted as Ant 1, with current distribution of 5 GHz is shown in Fig. 2(a). Strong currents exist on the feeding line and the arched edges. As well known, the radiation performance of antenna is generally based on the surface currents of metallic area. Thus, embedding CPW 2 in the area with weak currents will slightly influence the impedance bandwidth of CPW 1. To further study the influences of the CPW 2, antennas of the evolution processes are shown in Fig. 2(a), and the surface currents distributions at 5 GHz are also depicted in each antenna. Ant 2 is the transformation of Ant 1 by cutting the half slot out. The proposed MIMO antenna without band-notch structures and excitation of CPW 2 is denoted as Ant 3. As illustrated in Fig. 2, three antennas have similar current distributions at 5 GHz and slight discrepancies among three reflection coefficient curves, which indicates that three antennas obtain similar radiation characteristics. Thus, the influence of CPW 2 on CPW 1 can be ignored.

The ground plane of CPW 2 and the radiator of CPW 1 share a common metallic patch, and no decoupling structure is employed for good impedance matching. Thus, the orthogonally feeding structure is the sole method to achieve good isolation for our proposed MIMO antenna. This orthogonal structure also brings the features of pattern diversity and dual polarizations. The surface current and far-field distributions of two antenna elements are illustrated in Fig. 3 when two elements are

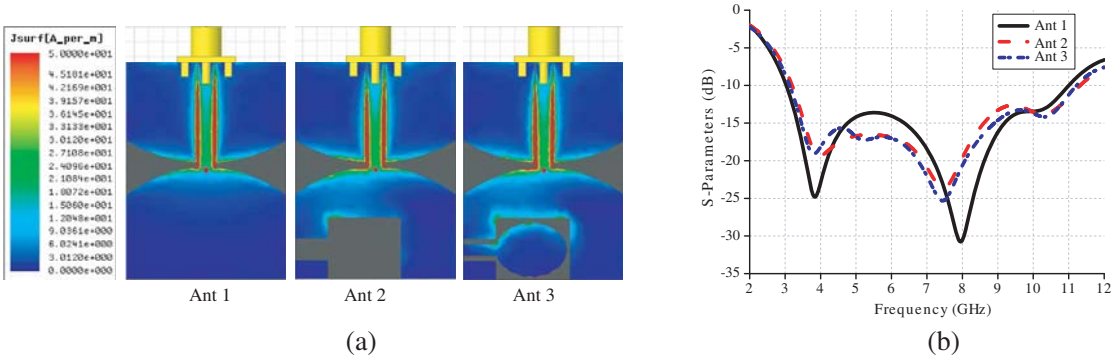

Figure 2. Ant 1 to Ant 3. (a) Current distribution of 5 GHz. (b) Simulated S-parameters.

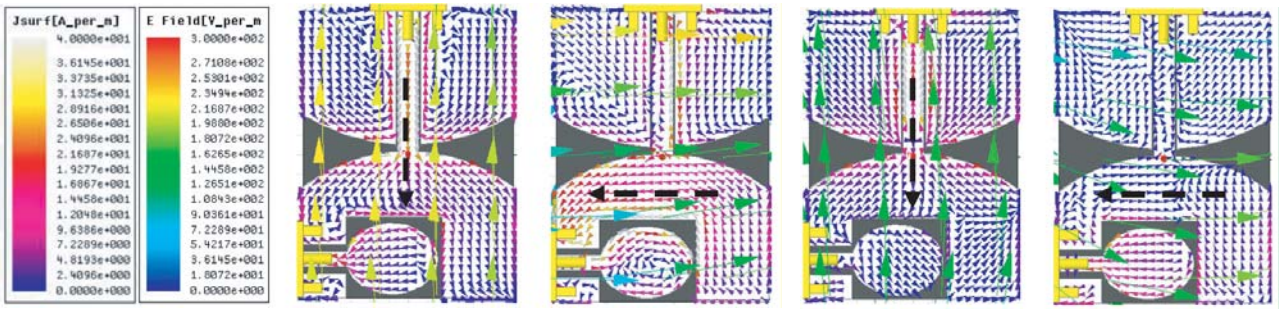

Figure 3. Simulated current and far field distributions. (a) CPW 1 at 3 GHz, (b) CPW 2 at 3 GHz, (c) CPW 1 at 10 GHz, (d) CPW 2 at 10 GHz. (The arrows with tail are far fields, without tail are surface currents. The black dotted arrow is.

excited independently. For CPW 1, it can be observed from Fig. 3(a) and (c) that the current vectors are enhanced along y-direction, and the current vectors of x-direction are canceled owning to the approximately symmetric structure. Thus, the main current direction of CPW 1 is parallel to y-axis. For CPW 2, its current vectors direction is primarily parallel to x-direction, and strong currents are coupled on the edges of the half slot as depicted in Figs. 3(b) and (d). Therefore, the orthogonal main currents of two elements achieve the perpendicular far fields and dual-polarization characteristic. Furthermore, the main current directions of two antenna elements remain unchanged independently of frequency due to the relatively stable current distributions. Thus, good isolation is achieved over the entire UWB frequency spectrum.

2.3. Band-Notch Structures

Four separate band-notch structures with a similar work mechanism are employed to eliminate the interference of 5.15–6 GHz. A T-shaped parasitic stub and a pair of C-shaped slots work as half-wavelength resonators while a rectangular slot and Z-shaped extended branch work as quarter-wavelength resonators. As aforementioned, these band-notch structures can be divided into two groups and filter the interference for CPW1 and CPW 2, respectively. The lengths of half-wavelength and quarter-wavelength resonators can be approximately calculated by formulas (1) and (2), respectively:

$$L_{\frac{\lambda_g}{2}} = \frac{c}{2 \times f_c \times \sqrt{\frac{1+\varepsilon_r}{2}}} \tag{1}$$

$$L_{\frac{\lambda_g}{4}} = \frac{c}{4 \times f_c \times \sqrt{\frac{1+\varepsilon_r}{2}}} \tag{2}$$

$L_{\frac{\lambda_g}{2}}$ / $L_{\frac{\lambda_g}{4}}$ is the length of the half-wavelength/quarter-wavelength resonator, c the speed of light in free space, ε_r the relative permittivity and f_c the centre frequency of notched band.

To prevent the rejection band from rapidly declining over the stop band, two resonators with separate center frequencies are employed. One is lower than 5.5 GHz and the other higher than 5.5 GHz. The optimizations of band-notch structures are shown in Fig. 4, and the optimal results are shown in Table 1. Notice that the length of the T-shaped stub is the half horizontal branch adding the vertical branch, and theoretical values in Table 1 are calculated through formulas (1) and (2). As observed, four different structures can realize the stop bands of 5–6 GHz except the Z-shaped branch, and all obtained stop bands decline rapidly out of center frequencies. For C-shaped slots and Z-shaped branch, impedance mismatching happens around 8 and 7 GHz, respectively, and thus only the antenna with these two structures cannot satisfy UWB applications. However, two band-notch structures in each group obtain separate center frequencies, which helps to construct new rejection bands by adding two structures to one antenna element. The simulated and measured S-parameters of the proposed antenna

Table 1. Optimal results of the band-notch structures.

	Length (mm)	Center Frequency(GHz)	Theoretical Value(mm)	Length/λ_g
T-shaped Stub	18.5	5.26	21.9	0.42
C-shaped Slots	19	5.97	19.3	0.49
Z-shaped Branch	9.9	5.32	10.8	0.23
Rectangular Slot	9.1	5.76	10.0	0.23

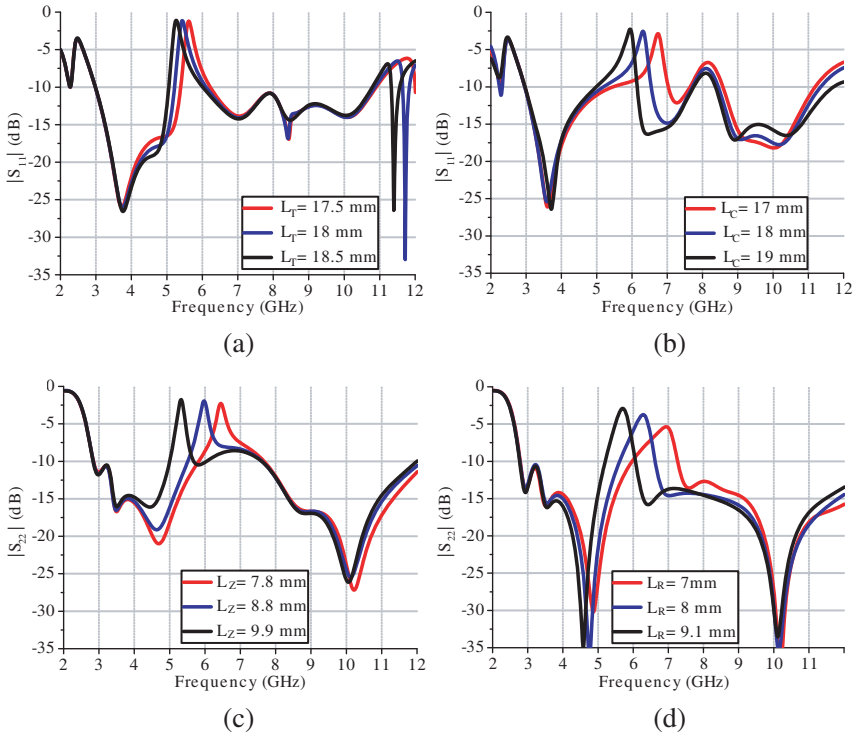

Figure 4. Optimizations of band-notch structures. (L_T, L_C, L_Z and L_R are the length of T-shaped stub, C-shaped slots, Z-shaped branch and Rectangular slot.). (a) T-shaped stub. (b) C-shaped slots. (c) Z-shaped branch. (d) Rectangular slot.

are illustrated in Fig. 5. When T-shaped stub and C-shaped slots are added simultaneously, a rejection band of 5–6 GHz is obtained, and the impedance matching around 8 GHz is improved. Compared with the sole band-notch structure, the new rejection band possesses relatively stable stop band, and it declines rapidly at cut-off frequencies. Similarly, a rejection band of 5–6 GHz with superior filter feature is obtained, and the impedance matching around 7 GHz is improved for CPW 2. Thus, the proposed antenna satisfies UWB applications, and the rejection bands with superior stopband characteristics are obtained for each antenna element.

To further study the band-notch characters, the current distributions are illustrated in Fig. 6. Figs. 6(a) and (b) are obtained when CPW 1 is excited, while Figs. 6(c) and (d) are obtained when CPW 2 is excited.

The T-shaped parasitic stub with symmetric configurations is added on the back of the substrate. The current path length of the stub is approximate to half wavelength. Its horizontal branch is near the arched edge of the radiator, and the vertical branch is on the center of the stripline, aiming at improving electromagnetic coupling and filter performance. The parasitic stub, resonating at 5.26 GHz, introduces

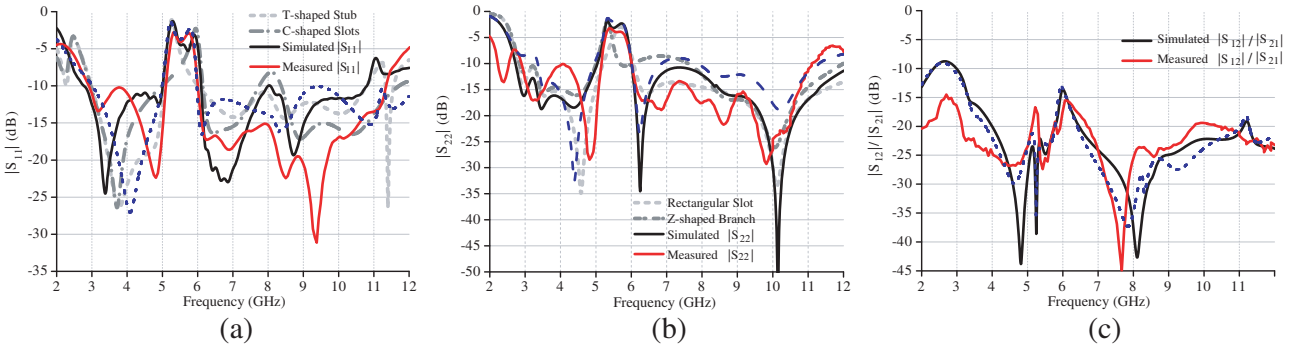

Figure 5. The simulated and measured S-parameters of proposed UWB MIMO antenna. (a) $|S_{11}|$. (b) $|S_{22}|$. (c) $|S_{12}|/|S_{21}|$.

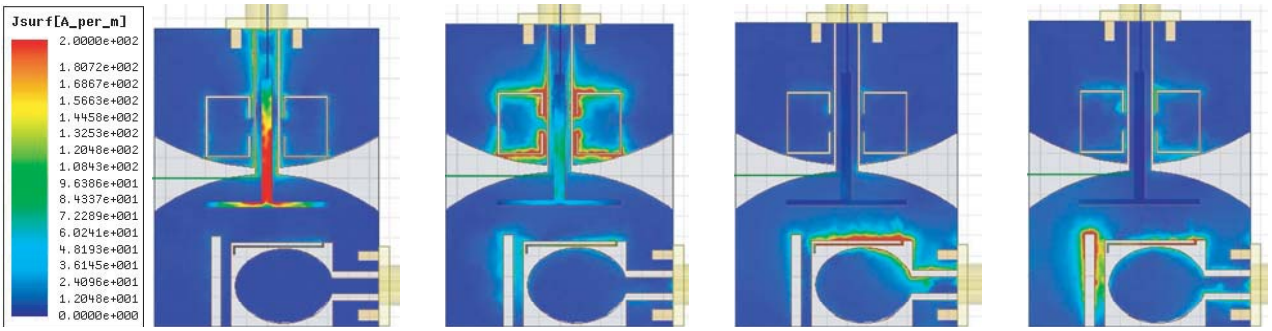

Figure 6. The simulated current distributions of proposed UWB MIMO antenna. (a) 5.26 GHz. (b) 5.97 GHz. (c) 5.32 GHz. (d) 5.76 GHz

an additional current path, and the induced currents on it have an opposite direction to those on the radiator and stripline of CWP 1, which significantly weakens the radiation. As shown in Fig. 5(a), the achieved rejection band with sharp shape declines rapidly (the light gray dashed line). To achieve good stop-band characteristic, a pair of C-shaped slots is employed and symmetrically notched on the top of the ground plane of CPW 1 near the stripline, which generates a new resonance at 5.97 GHz. Strong surface currents are coupled around the slots, and half-wavelength currents are also found along the slots. Thus, total effective radiation recedes ulteriorly. As seen in Figs. 6(a) and (b), very weak currents distribute around the Z-shaped branch and rectangular slot when only CWP 1 is excited, because the currents mainly concentrate on the stripline and the arched edges of CPW 1 as depicted in Fig. 2(a), and then the electromagnetic energy is prone coupling to T-shaped stub and C-shaped slots. Thus, this band-notch group primarily works for CPW 1.

For CPW 2, the Z-shaped branch with length of 9.9 mm is introduced. A rejection band of 5–5.6 GHz is achieved with resonant frequency of 5.32 GHz. Strong currents distribute on the branch, and quarter-wavelength current is along the branch as shown in Fig. 6(c). However, the impendence matching of 5.6–7.5 GHz deteriorates as seen in Fig. 5(b) (the dark gray dash-dotted line). A simple open-ended rectangular slot is notched on the top of the half slot. As depicted in Fig. 6(d), strong currents concentrate on the rectangular slot and the Z-shaped branch at 5.76 GHz. Because the slot, which is between the Z-shaped branch and the ground plane of CPW 2, has a similar length to the rectangular slot, when two structures are added simultaneously, a relatively stable stop band with sharp edges is obtained, and the impendence matching of 6–7.5 GHz is below -10 dB. As aforementioned, the currents mainly concentrate on the half slot when CPW 2 is excited, and then weak currents distribute on the T-shaped stub and C-shaped slots. Therefore, the Z-shaped branch and rectangular slot primarily filter the interferences for CPW 2.

3. RESULTS AND DISCUSSION

3.1. Impedance Performance

As depicted in Fig. 5, the measured impedance bandwidths are 2.8–5 and 6.1–11.3 GHz for $|S_{11}|$, 2.9–5.16 and 6–11.1 GHz for $|S_{22}|$. The measured mutual coupling is below −15 dB over the entire UWB frequency spectrum band (most below −20 dB). The discrepancies between simulations and measurements are acceptable. Some discrepancies happen due to the errors of fabrication and measurement tolerance. Notice that the blue dashed lines in Fig. 5 are obtained using wave ports in simulations. Compared with the measured results, some resonant frequencies disappear, e.g., 3–5 GHz in Fig. 5(a), and large disagreements happen, e.g., 3–4 and 7–9 GHz in Fig. 5(b). Thus, the simulated results (dark line) using SMA model can decrease the errors in the software simulations.

3.2. Radiation Performance

Due to the available hardware (the measured range of our workable Satimo anechoic chamber is from 0.8 to 6 GHz), the radiating performance of 2–6 GHz is measured by Satimo anechoic chamber, and the results of 6–12.4 GHz are simulated by software. The radiation patterns, in *xoz* and *yoz* plane, of the proposed antenna are illustrated in Fig. 7 when one port is excited and the other port terminated with 50 Ohm load. CPW 1 possesses the radiating patterns with dumb-bell shape in *yoz* plane (E face) and relatively stable omnidirectional radiation patterns in the *xoz* plane (H face), while CPW 2 has similar radiation patterns to CPW 1 in the contrary planes. In other words, *xoz* plane is the E face, and *yoz* plane is the H face for CPW 2. Thus, the proposed MIMO antenna realizes pattern diversity. It can be observed that the *H*-plane of CPW 2 is slightly directional, toward $\varphi = 270°$, resulting from the reflective effect of the ground plane of CPW 1. As found in Fig. 7, two antenna elements cannot effectively radiate at 5.3 and 5.4 GHz, and then the radiating energy is obviously weaker than that at other frequencies.

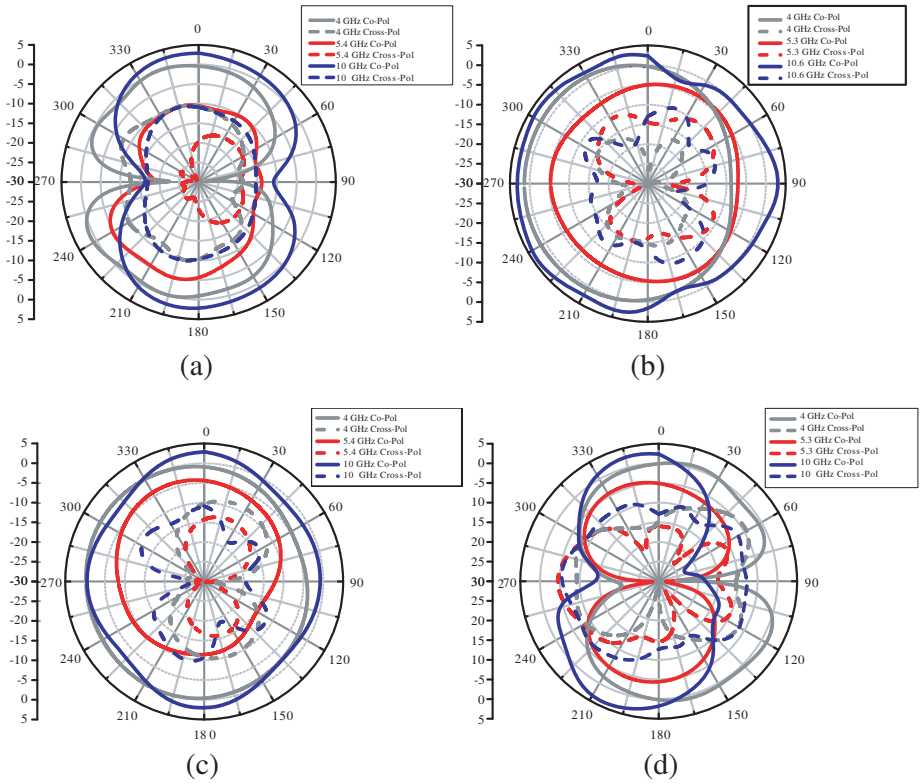

Figure 7. 2-D radiation patterns. (a) *yoz* plane of CPW 1. (b) *yoz* plane of CPW 2. (c) *xoz* plane of CPW 1. (d) *xoz* plane of CPW 2.

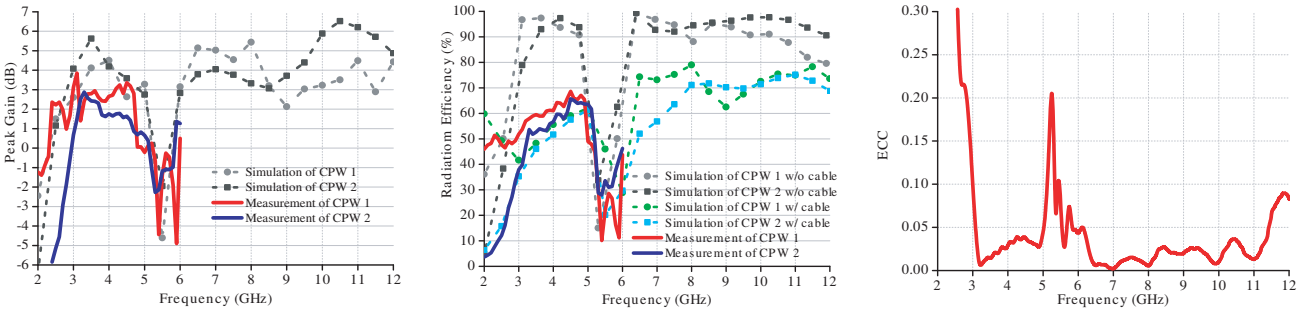

Figure 8. Far field characters. (a) Peak gain. (b) Radiation efficiency. (c) Envelope correlation coefficient.

The peak gains and radiation efficiency of the proposed antenna are described in Figs. 8(a) and (b). For CPW 1, the peak gain ranges from 2 to 6 dBi over the entire UWB frequency band, and a notch band with minimum value of −5 dBi is found from 5 to 6 GHz. For CPW 2, the peak gain ranges from 3 to 7 dBi, and a notch band with minimum value of −2.5 dBi is also found from 5 to 6 GHz. The radiation efficiencies of the proposed antenna elements are above 80%, and they decrease significantly at the notch bands. In the practical measurements, an extra feeding cable is utilized to connect antenna to the measurement system, and the cable is covered with EMI suppressant material. For our proposed MIMO antenna, the ground plane of each element is electrically small at lower frequency, and then some induced currents on the outer surface of the cable cause the secondary radiations. However, most radiated energy is absorbed by the EMI suppressant material. Thus, large discrepancies between the no cable simulated radiation efficiencies and the measured ones appear, and the measured gains are also smaller than the simulated results. To verify the analysis, the simulated radiation efficiency with cable is shown in Fig. 8(b). The simulated results with cable have good agreement with the measured ones, and the discrepancies between two kinds of simulations (with and without cable) decrease at higher frequency due to the much less induced currents.

3.3. Envelope Correlation Coefficient

Envelope correlation coefficient (ECC) depicts the extent of isolation or correlation of different communication channels. For the proposed MIMO antenna, ECC can be calculated by [7] (1). As illustrated in Fig. 8(c), the measured ECC values are below 0.05 over the entire UWB frequency except 5–6 GHz. Thus, the proposed MIMO antenna achieves good diversity performance.

4. CONCLUSION

A new method to reduce the overall dimension of UWB MIMO antenna is presented in this paper. The overall size is totally decided by CPW 1, while CPW 2 is fabricated in the radiating patch of CPW 1. Two groups of band-notch structures efficiently eliminate the interference of 5.15–6 GHz, and they work independently for separate antenna elements. The measured results show that the impedance bandwidths of the proposed antenna are wider than UWB application frequency band, and the mutual coupling is less than −15 dB (most below −20 dB) due to its orthogonally feeding structure. There are no extra decoupling structures to be designed, which significantly economizes the space and simplifies the design processes. The proposed MIMO antenna also possesses stable radiation patterns, high radiation efficiency and low ECC values. Thus, these measurements and superiorities of the proposed antenna demonstrate that it is a competitive candidate for UWB applications.

ACKNOWLEDGMENT

This work was supported by the National Natural Science Foundation of China (NNSF) under Grants 61531016 and 61271090, and Science and Technology Foundation of Sichuan Province under Grants 2015GZ0103 and 2016GZ0059.

REFERENCES

1. FCC, "First report and order," 2002.
2. Lim, A. W. C. and V. K. N. Lau, "On the fundamental tradeoff of spatial diversity and spatial multiplexing of MIMO links with imperfect CSIT," *ISIT 2006*, Seattle, USA, July 9–14, 2006.
3. Mao, C.-X. and Q.-X. Chu, "Compact coradiator UWB-MIMO antenna with dual polarization," *IEEE Trans. Antennas Propag.*, Vol. 62, 4474–4480, 2014.
4. Zhu, J., S. Li, et al., "Compact dual polarized UWB quasi-self-complementary MIMO/diversity antenna with band-rejection capability," *IEEE Antennas Wireless Propag. Lett.*, Vol. PP, 1–1, 2015.
5. Ren, J., W. Hu, Y. Yin, and R. Fan, "Compact printed MIMO antenna for UWB applications," *IEEE Antennas Wireless Propag. Lett.*, Vol. 13, 1517–1520, 2014.
6. Gao, P., S. He, et al., "Compact printed UWB diversity slot antenna with 5.5-GHz band-notched characteristics," *IEEE Antennas Wireless Propag. Lett.*, Vol. 13, 376–379, 2014.
7. Kang, L., H. Li, et al., "Compact offset microstrip-fed MIMO antenna for band-notched UWB application," *IEEE Antennas Wireless Propag. Lett.*, Vol. 14, 1754–1757, 2015.
8. Tang, T.-C. and K.-H. Lin, "An ultrawideband MIMO antenna with dual band-notched function," *IEEE Antennas Wireless Propag. Lett.*, Vol. 13, 1076–1079, 2014.
9. Li, Q., A. P. Feresidis, et al., "Miniaturized double-layer EBG structures for broadband mutual coupling reduction between UWB monopoles," *IEEE Trans. Antennas Propag.*, Vol. 63, 1168–1171, 2015.
10. Zhang, S. and G. F. Pedersen, "Mutual coupling reduction for UWB MIMO antennas with a wideband neutralization line," *IEEE Antennas Wireless Propag. Lett.*, Vol. PP, 1–1, 2015.
11. Zhang, S., B. K. Lau, A. Sunesson, et al., "Closely-packed UWB MIMO/diversity antenna with different patterns and polarizations for USB dongle applications," *IEEE Trans. Antennas Propag.*, Vol. 60, 4372–4380, 2012.